RSC Advances

In-situ Constructing α-Bi2O3/g-C3N4/β-Bi2O3 Composites and Their Highly Efficient Photocatalytic Performances

Journal:	*RSC Advances*
Manuscript ID	RA-ART-09-2015-018420.R1
Article Type:	Paper
Date Submitted by the Author:	03-Oct-2015
Complete List of Authors:	Jiang, Haiying; Renmin University, Chemistry Liu, Guigao; National Insititute for Materials Science, Research Unit for Enviromental Remediation Materials Science Wang, Tao; National Insitute for Materials Science, Research Unit for Enviromental Remediation Materials Science Li, Peng; National Institute for Materials Science, Ye, Jinhua; National Institute for Materials Science, Lin, Jun; Renmin University of China, Chemistry
Subject area & keyword:	Photocatalysis < Catalysis

Journal Name

ARTICLE

In-situ Constructing α-Bi_2O_3/g-C_3N_4/β-Bi_2O_3 Composites and Their Highly Efficient Photocatalytic Performances

Received 00th January 20xx,
Accepted 00th January 20xx

DOI: 10.1039/x0xx00000x

www.rsc.org/

Hai-Ying Jiang[a, b], Guigao liu[b], Tao Wang[b], Peng Li[b], Jun Lin*[a], and Jinhua Ye*[b]

In this study, α-Bi_2O_3/g-C_3N_4/β-Bi_2O_3 composites were constructed by an in-situ method in one step by α-Bi_2O_3 and g-C_3N_4. It indicates that α-Bi_2O_3 transformed to β-Bi_2O_3 when it was calcined with g-C_3N_4 together. The co-existences of α-Bi_2O_3, g-C_3N_4 and β-Bi_2O_3 were proved by X-ray diffraction (XRD), Fourier transform infrared (FT-IR) spectroscope and high-resolution transmission electron microscope (HRTEM). The energy band structures and optical properties were studied by ultraviolet-visible diffuse reflectance spectroscope (UV-vis DRS) and Valence band X-ray photoelectron spectroscope (VB-XPS). The in-situ formation mechanism of α-Bi_2O_3/g-C_3N_4/β-Bi_2O_3 composites in one step was studied by the samples' surface chemical states, which were measured by X-ray photoelectron spectroscope (XPS). The results show that the surface covered or coordinated g-C_3N_4 and CO_3^{2-} have promotional effect on the stability of β-Bi_2O_3 at room temperature. The enhanced photocatalytic activities of α-Bi_2O_3/g-C_3N_4/β-Bi_2O_3 composites were evaluated by the photocatalytic oxidation of isopropyl alcohol (IPA), and attributed to the heterojunction formation between β-Bi_2O_3 and g-C_3N_4.

Introduction

TiO_2 has been developed to be a famous photocatalyst since the discovery of photocatalytic splitting of water molecular on TiO_2 electrode in 1972[1]. However, its practical application is greatly hindered by its only UV light response. From the view of effectively utilizing the solar light, visible-light-responsive photocatalysts are attracting increasing interests in the recent years. Bi_2O_3 semiconductors are a serious of visible-light-responsive photocatalysts with appropriate band gaps[2]. Up to now, six polymorphic forms have been found in this family, monoclinic α-phase, tetragonal β- phase, body- centered cubic γ- phase, face-centered cubic δ- phase, tetragonal ε- phase, and triclinic ω- phase[3]. Among them, α-Bi_2O_3 and β-Bi_2O_3 were mostly studied in the past because of their respective highest thermal stability and photocatalytic activity[2, 4-13].

α-Bi_2O_3 is an attractive photocatalyst because of its easy preparation[10], environmental friendship and thermal stability[14-18]. However, its photocatalytic activity has been proved to be poor due to its some unfavorable properties for photocatalysis, although it has some properties beneficial for photocatalysis, such as narrow band gap (+ 2.8 eV), high valence band potential (+ 3.13 V *vs*. NHE)[19], etc. Firstly, its conduction band potential (+ 0.33 V *vs*. NHE) is too low to oxide the surface O_2 to O_2^- (- 0.33 V *vs*. NHE) through a fast single-electron reaction, resulting in a high recombination rate of the photogenerated electrons and holes[14, 20]. Secondly, the particle size of α-Bi_2O_3 prepared by usual methods is very large (dozens of micrometers), resulting in low surface areas[9, 10, 21]. Therefore, developing useful strategies to improve the photocatalytic activity of α-Bi_2O_3 is the main research point in this field.

The construction of heterojunctions is a mostly used method to improve the photocatalytic activity in the last decades[4, 6, 22, 23]. g-C_3N_4 is a typical, polymeric and graphical layered material; its photocatalytic activity is poor due to its high photocarriers' recombination rate[24-26]. Therefore, it is often regarded as a good candidate for the construction of heterojunctions. However, this work is one of the accidents in the heterojunction construction process of α-Bi_2O_3 and g-C_3N_4, while the other accident has been reported by us recently[19]. In this work, both morphology and crystal structure of α-Bi_2O_3 have great changes in this process. Here, we will mainly discuss the crystal structure changes of α-Bi_2O_3, sine the morphology changes has been discussed detailedly in another paper[19].

In this study, α-Bi_2O_3/g-C_3N_4/β-Bi_2O_3 composites were successfully constructed by α-Bi_2O_3 and g-C_3N_4 in one step with an in situ method. Components of the prepared samples were studied by X-ray diffraction (XRD) and Fourier transform infrared (FT-IR) spectroscopy. Morphologies of the composites were recorded by field-emission scanning electron microscope (FE-SEM), transmission electron microscope (TEM), and high-resolution transmission electron microscope (HRTEM). The energy band structures and optical properties were studied by ultraviolet-visible diffuse reflectance spectroscope (UV-vis DRS) and Valence band X-ray photoelectron spectroscopy (VB-XPS). The in-situ formation mechanism of α-Bi_2O_3/g-C_3N_4/β-Bi_2O_3 composites in one step was studied by the samples' surface chemical states, which were measured by X-ray photoelectron spectroscope (XPS). The

[a] Department of Chemistry, Renmin University of China, Beijing 100872, People's Republic of China E-mail: jin@chem.ruc.edu.cn; Fax: +86-10-62516444; Tel: +86-10-62514133
[b] Environmental Remediation Materials Unit and International Center for Materials Nanoarchitectonics (WPI-MANA), National Institute for Materials Science (NIMS), 1-1, Namiki, Tsukuba, Ibaraki 305-0044, Japan Email: Jinhua.YE@nims.go.jp; Fax: +81-29-860-4958; Tel: +81-29-859-2646

photocatalytic activity enhancement of α-Bi_2O_3/g-C_3N_4/β-Bi_2O_3 composites were also studied by the photocatalytic oxidation of IPA, and discussed in detail in this work.

Experimental

2.1 Sample preparation

The micro-rod like α-Bi_2O_3 was prepared by a precipitation method using $Bi(NO_3)_3$ as the Bi source[10, 27]. Typically, 10.78 g of $Bi(NO_3)_3 \cdot 5H_2O$ was dissolved in a 30 mL aqueous solution of HNO_3 (1.5 M) at first, to avoid the hydrolyzation of Bi^{3+} ions. Secondly, the NaOH solution (50% w/v) was added into the solution dropwise until pH > 13, under vigorous agitation. In that process, yellow precipitate was formed. Thirdly, the suspension was heated to 80 °C and kept for 2 hours, and the precipitate was subsequently collected by centrifugation and being washed with deionized water several times. After that, the resultant solid was dried at 120 °C overnight in air. Lastly, the powder was calcined at 450 °C for 5 hours.

The g-C_3N_4 was synthesized by heating the melamine at 520 °C for 4 hours in a half-open system, according to the previous report[28].

The α-Bi_2O_3/g-C_3N_4/β-Bi_2O_3 composites were constructed according to our earlier research as follows[29, 30]: the g-C_3N_4 and microrod-like α-Bi_2O_3 with different weight fractions were thrown into 100 ml alcohol (95%), following with 3 hours' ultrasonication and 24 hours' stirring at room temperature. Before the last calcinations at 450 °C in a half-open system, the products were dried at 100 °C for 12 hours in advance. The weight ratios of g-C_3N_4 and micro-rod α-Bi_2O_3 were represented by n_1 : n_2. The calcination time was set to be 3 hours, 4 hours and 5 hours.

Moreover, the nano α-Bi_2O_3 and β-Bi_2O_3 were synthesized for comparison, using the $Bi_2O_2CO_3$ as a precursor [31].

2.2 Characterizations

The crystal structures of the precursor and Bi_2O_3 samples were determined with an X-ray diffractometer (X'pert Powder, PANalytical B. V., Netherlands) with Cu - Kα radiation. The IR absorption spectra were obtained with a Fourier transform-infrared (FT-IR) spectrophotometer (IRPrestige-21, Shimadzu Co., Japan). Field-emission electron microscopy (FESEM) was performed to observe the morphologies on a JEOL 6701F microscope. High-resolution transmission electron microscope images were recorded with a high-resolution transmission electron microscope (HRTEM, Tecnai G2F30). The diffuse reflection spectra were measured with an integrating sphere equipped ultraviolet-visible (UV-vis) recording spectrophotometer (UV-2500PC, Shimadzu Co., Japan) using $BaSO_4$ as reference and the optical absorption spectra were converted from the diffuse reflection spectra according to the Kubelka-Munk equation. X-ray photoelectron spectroscopy (XPS) was performed on an ESCALAB 250Xi spectrometerequipped with 300W Al Kα radiation, while all binding energies were referenced to the C1s peak (284.6 eV) of the surface adventitious carbon.

2.3 Photocatalytic Activity

The photocatalytic oxidations of gaseous IPA were carried out to evaluate the photocatalytic activities of α-Bi_2O_3/g-C_3N_4/β-Bi_2O_3 composites. The experiments were carried out under the visible light irradiation (420 nm ≤ λ ≤ 800 nm). The light source was a 300 W Xe-arc lamp (10 A imported current, focused through a 50 × 50 mm^2 shutter window) equipped with wavelength cut-off filters and a water filter. 50 mg of α-Bi_2O_3/g-C_3N_4/β-Bi_2O_3 powder was bespread uniformly on a glass dish with an area of 9 cm^2. A certain amount of gaseous IPA (~1400 ppm) was injected into the vessel and kept for 2 hour in the dark before irradiation. During the irradiation by visible light, 0.5 ml of the gas was sampled everyone 1 hour intervals. The products were analyzed with a gas chromatograph (GC-2014, Shimadzu, Japan) with a flame ionization detector (FID). Meanwhile, the g-C_3N_4, nano α-Bi_2O_3 and β-Bi_2O_3 were also used to photooxide the IPA for comparison under the same conditions. Furthermore, the adsorptions of IPA in dark over α-Bi_2O_3/g-C_3N_4/β-Bi_2O_3 composites were also carried out without light irradiation.

Results and discussion

3.1 Components of α-Bi_2O_3/g-C_3N_4/β-Bi_2O_3 composites

The components of the prepared α-Bi_2O_3/g-C_3N_4/β-Bi_2O_3 composites were identified by XRD and FT-IR spectra.

The crystal structures of the composites were identified by XRD pattern in Fig. 1. All the samples were compared with the ICSD file of No. 41-1449 and No. 27-0053, respectively corresponding to α-Bi_2O_3 and β-Bi_2O_3[32]. The results indicate that, the crystal structures obviously changed with the increase of the weight ratio of g-C_3N_4 in the mixture of α-Bi_2O_3/g-C_3N_4, as well as the calcination time. Firstly, with the increase of the weight ratio of g-C_3N_4, we found that the characteristic peaks of β-Bi_2O_3 become more and more strong, evidences that α-Bi_2O_3 gradually changes to β-Bi_2O_3. Then for the sample of 9.5:0.5, when the calcination time prolonged from 3 hours to 4 hours, almost no characteristic peaks of α-Bi_2O_3 is observed in the XRD spectrum; when the calcination time was further prolonged to 5 hours, the characteristic peaks of α-Bi_2O_3 appear again. The XRD results show that both α-Bi_2O_3 and β-Bi_2O_3 exist in the composites. However, we can't see any characteristic peaks derived from g-C_3N_4 in the XRD spectra, so we can't get any information of g-C_3N_4 by XRD. Therefore, the FT - IR was used to prove the existence of g-C_3N_4 in the composite samples. As shown in Fig. 2, we can clearly see the vibration peaks (820 cm^{-1}, 890 cm^{-1}, 1000-1900 cm^{-1}, 1965 cm^{-1}, 2054 cm^{-1}, 2141 cm^{-1}, and 2800-3700 cm^{-1}) derived from g-C_3N_4 in all the composite samples.

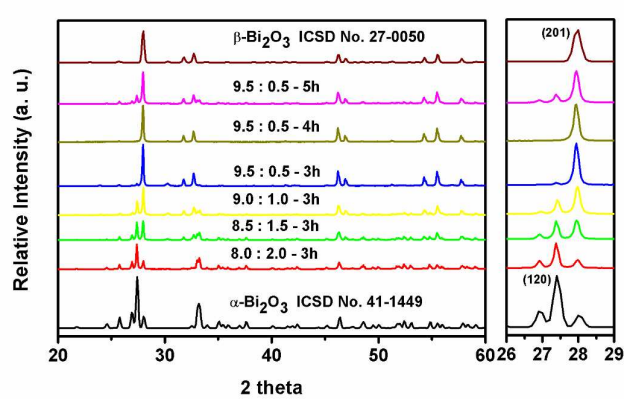

Fig. 1 XRD spectra of all the α-Bi_2O_3/g-C_3N_4/β-Bi_2O_3 composite samples

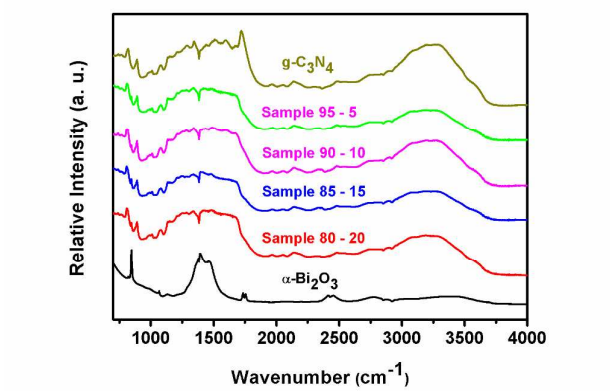

Fig. 2 FT-IR absorption spectra of all the α-Bi_2O_3/g-C_3N_4/β-Bi_2O_3 composite samples

Detailedly, we also measure the practical weight ratios of the respective α-Bi_2O_3, β-Bi_2O_3 and g-C_3N_4, in α-Bi_2O_3/g-C_3N_4/β-Bi_2O_3 composites. The weight ratios of the g-C_3N_4 were measured through the mass discrepancy before and after the calcination process of every α-Bi_2O_3/g-C_3N_4 mixture samples, because the g-C_3N_4 will dissolves in the presence of a second phase during the calcination processes at 450 ^oC. The contents of α-Bi_2O_3 and β-Bi_2O_3 in the sequence of as-prepared composites, were obtained by simulating the XRD pattern with standard crystal structures of α-Bi_2O_3 and β-Bi_2O_3, through a Maud program[33]. The results were displayed in Table 1.

Table 1 Contents of the α-Bi_2O_3/g-C_3N_4/β-Bi_2O_3 composites

Content / Weight Fraction (%) / Sample	α-Bi_2O_3	β-Bi_2O_3	g-C_3N_4
α-Bi_2O_3	100	-	-
β-Bi_2O_3	-	100	-
8.0:2.0-3h	91.15	8.85	<0.100
8.5:1.5-3h	58.20	33.74	8.060
9.0:1.0-3h	37.86	57.24	4.900
9.5:0.5-3h	1.350	18.46	80.19
9.5:0.5-4h	1.150	47.41	51.44
9.5:0.5-5h	14.16	61.84	24.00
g-C_3N_4	-	-	100

3.2 Micro-morphologies and structures

As we reported in the earlier research, the morphologies of α-Bi_2O_3 was significantly changed when it was heat treated with g-C_3N_4 together[19]. In this study, the morphologies of the composites were observed by FE-SEM, as shown in Fig. 3. We found that the morphologies of both α-Bi_2O_3 and g-C_3N_4 have huge changes. As we can see that, the particle size of Bi_2O_3 decreased from micrometer to nanometer, which is the same with our previous report[19]. The size of g-C_3N_4 also has some decrease. The mechanism of the morphology changes has been explained in our earlier report[19].

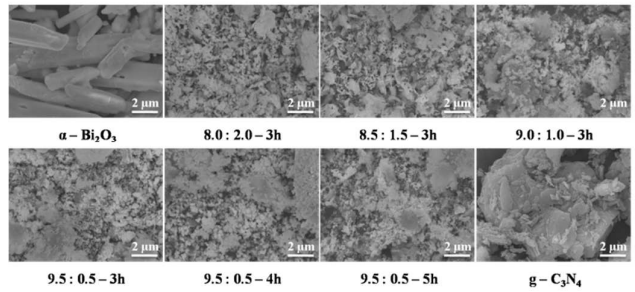

Fig. 3 SEM images of all the α-Bi_2O_3/g-C_3N_4/β-Bi_2O_3 composite samples

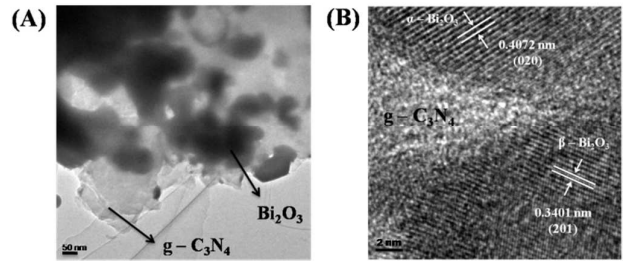

Fig. 4 TEM (A) and HRTEM (B) images of the α-Bi_2O_3/g-C_3N_4/β-Bi_2O_3 composite samples (9.5 : 0.5 - 3h)

Further, layered structures of g-C_3N_4 were observed in Fig. 4 (A) with TEM, and Bi_2O_3 particles were packaged in the g-C_3N_4 nanosheets. From the HRTEM image in Fig. 4 (B), we can clearly see the coexistence of α-Bi_2O_3, β-Bi_2O_3 and g-C_3N_4. The amorphous fraction is identified to be g-C_3N_4 nanosheets; the lattice space of 0.4072 nm is attributed to the (020) facet of α-Bi_2O_3; the lattice space of 0.3401 nm is accordance with the (201) crystal planes of β-Bi_2O_3. The TEM and HRTEM images indicate the co-existence of α-Bi_2O_3, β-Bi_2O_3 and g-C_3N_4, as well as good contacts between any two phases of them. In addition, the SEM spectra of nano α-Bi_2O_3 and β-Bi_2O_3 are also displayed in Fig. S1.

3. 3 Energy band structures and optical properties

The energy band structures of α-Bi_2O_3, β-Bi_2O_3 and g-C_3N_4 were studied by the combinations of UV-vis DRS and VB-XPS.

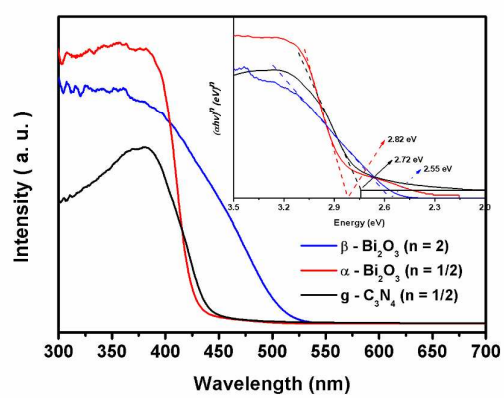

Fig. 5 UV-vis absorption spectra of the as-prepared α-Bi_2O_3, g-C_3N_4 and β-Bi_2O_3; the insets are the corresponding Tauc Plots curves

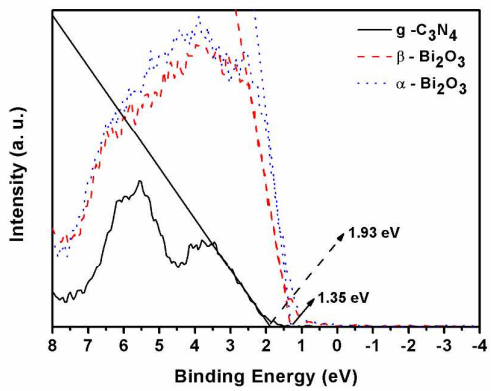

Fig. 6 VB-XPS spectra of the as-prepared α-Bi_2O_3, g-C_3N_4 and β-Bi_2O_3

The band gaps of α-Bi_2O_3, β-Bi_2O_3 and g-C_3N_4 were obtained from a Tauc plot spectra, which was transferred from the UV-vis DRS spectra (Fig. 5) through Tauc equation as follows[18]:

$$(\alpha h\nu)^n = A\,(h\nu - E_g)$$

In this equation, α, ν, A and E_g are the absorption coefficient, light frequency, proportionality constant and band gap. The value of the index n depends on the property of the materials: for the direct band-gap semiconductors, n = 2; for the indirect band-gap semiconductors, n = 1/2. According to the earlier literatures, α-Bi_2O_3[34]and g-C_3N_4[28]are indirect band-gap semiconductors; β-Bi_2O_3[35]is direct band-gap semiconductor. Therefore, the value of n is determined to be 1/2 for α-Bi_2O_3 and g-C_3N_4, and 2 for β-Bi_2O_3. Based on the results, the Tauc plot spectra of $(\alpha h\nu)^n$ *vs.* photo energy is described as the inset of Fig. 5 The band gaps of α-Bi_2O_3, β-Bi_2O_3 and g-C_3N_4 were estimated to be 2.82 eV, 2.55 eV and 2.72 eV, from the tangent lines.

The energy differences between the Fermi levels and valence bands of α-Bi_2O_3, β-Bi_2O_3 and g-C_3N_4 were measured by VB-XPS (Fig. 6). As shown in Fig. 6, the energy differences between the Fermi levels and valence bands of α-Bi_2O_3 and β-Bi_2O_3 are almost the same, and the value is + 1.35 eV, while this value of g-C_3N_4 is + 1.93 eV. According to the literatures, the Fermi levels of α-Bi_2O_3, β-Bi_2O_3 and g-C_3N_4 are respective +1.73 eV[36], + 0.54 eV[6] and - 0.3 eV[37].

Combing the values of band gaps, Fermi levels and the energy differences between Fermi level and valence bands, we obtained the energy band structures of α-Bi_2O_3, β-Bi_2O_3 and g-C_3N_4. The specific values are displayed in Table 2.

Table 2 Energy band structures of α-Bi_2O_3, β-Bi_2O_3 and g-C_3N_4

Contents / Values / Sample	Band gap (eV)	Valence band (eV vs. NHE)	Conduction band (eV vs. NHE)	Fermi Level (eV vs. NHE)
α-Bi_2O_3	2.82	+ 3.08	+ 0.26	+ 1.73
g-C_3N_4	2.72	+ 1.63	- 1.09	+ 0.54
β-Bi_2O_3	2.55	+ 1.89	- 0.66	- 0.30

The optical absorption spectra of α-Bi_2O_3/g-C_3N_4/β-Bi_2O_3 composites were studied by UV-vis DRS spectra (Fig. 7). We found that with the weight ratio decrease of α-Bi_2O_3 in α-Bi_2O_3/g-C_3N_4/β-Bi_2O_3 composites, the visible light absorption intensity during 420 nm to 550 nm has gradual increase and a red shift. According to the UV-vis DRS results, the light absorption region is greatly enhanced by the constructions of α-Bi_2O_3/g-C_3N_4/β-Bi_2O_3 composites.

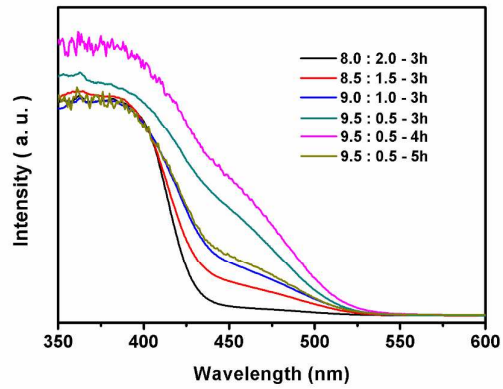

Fig. 7 UV-vis absorption spectra of the α-Bi_2O_3/g-C_3N_4/β-Bi_2O_3 composite samples

3.4 Formation Mechanism

As we know, β-Bi_2O_3 is not stable at room temperature, but it is formed in this work. It was reported that, the surface-coordinated organic ligands and CO_3^{2-} can lower the surface energy of $NaNbO_3$ and make it stable at room temperature[38]. Therefore, we speculate that the CO_3^{2-} and g-C_3N_4 have the same effect for the stabilization of β-Bi_2O_3 at room temperature.

In order to understand the formation mechanism of α-Bi_2O_3/g-C_3N_4/β-Bi_2O_3 composites and prove our speculation, we studied the surface chemical states of the composite samples, g-C_3N_4 and α-Bi_2O_3 by XPS spectra. In Fig. 8, the high resolution XPS spectra of C1s, N1s, Bi4f and O1s were studied in detail. From Fig. 8 (A), two type of carbon were observed in all the three samples. For α-Bi_2O_3, the two types of carbon were attributed to the surface adventitious carbon (286.4 eV) and carbon in CO_3^{2-} group (288.261 eV), according to the earlier literatures[39, 40]. For g-C_3N_4 and α-Bi_2O_3/g-C_3N_4/β-Bi_2O_3 composite, the two types of carbon were attributed to the surface adventitious carbon (286.4 eV) and g-C_3N_4[25] (287.935 eV and 287.985 eV). From Fig. 8 (B), three types of nitrogen were observed in the samples of g-C_3N_4 and α-Bi_2O_3/g-C_3N_4/β-Bi_2O_3 composite, and they are all derived from g-C_3N_4. They are respectively assigned to tertiary nitrogen [N-$(C)_3$] groups (398.443 eV and 398.489 eV), sp^2-hybridized nitrogen (=NH, -NH_2) (399.964 eV and 400.147 eV), and the charging effects (404.228 eV and 404.326 eV)[25]. In Fig. 8 (C), the characteristic peaks of Bi^{3+} were observed in both the α-Bi_2O_3 and α-Bi_2O_3/g-C_3N_4/β-Bi_2O_3 composite samples, and ascribed as $Bi4f_{5/2}$ (163.786 eV and 163.889 eV)and $Bi4f_{7/2}$ (158.479 eV and 158.583 eV)[22]. In Fig. 8 (D), the three peaks of oxygen in the samples of α-Bi_2O_3 and α-Bi_2O_3/g-C_3N_4/β-Bi_2O_3 composite were attributed to Bi - O - Bi[21] (529.385 eV and 530.817 eV), CO_3^{2-} group (530.540 eV and 529.817 eV) [41]and H - O - H (532.234 eV)[42], while only H - O - H coordination peak of oxygen was observed in g-C_3N_4 samples. Meanwhile, the CO_3^{2-} on the surface of α-Bi_2O_3/g-C_3N_4/β-Bi_2O_3 composite sample (52%) is higher than that of α-Bi_2O_3 (36%). In addition, we also found that

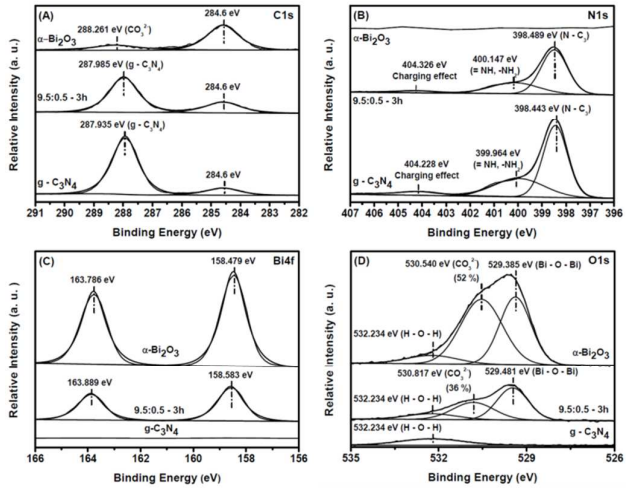

Fig. 8 XPS spectra of (A) C1s; (B) N1s; (C) Bi4f; (D) O1s for α-Bi_2O_3, α-Bi_2O_3/g-C_3N_4/β-Bi_2O_3, and g-C_3N_4

the binding energies of all the peaks in α-Bi_2O_3/g-C_3N_4/β-Bi_2O_3 composite sample are slightly higher than those in α-Bi_2O_3 or g-C_3N_4, except the C1s of surface adventitious carbon and O1s of H - O - H. This is probably because of the interaction between α-Bi_2O_3, β-Bi_2O_3 and g-C_3N_4. The XPS results indicate the co-existence of g-C_3N_4 [Fig. 8 (A)] and CO_3^{2-} [Fig. 8 (D)] on the surface of α-Bi_2O_3/g-C_3N_4/β-Bi_2O_3 composites.

As a result, we proposed the formation mechanism of α-Bi_2O_3/g-C_3N_4/β-Bi_2O_3 composites as described in Scheme 1. Step 1: α-Bi_2O_3 transfers to β-Bi_2O_3 at the temperature of 450 °C, while g-C_3N_4 slowly dissolves into CO_2 at about 400 °C[19]; Step 2: The released CO_2 corrodes the surfaces of the microrod-like α-Bi_2O_3 by reacting with it, and produces $Bi_2O_2CO_3$, forming g-C_3N_4/$Bi_2O_2CO_3$ composite; Step 3: The $Bi_2O_2CO_3$ crystals further decompose into β-Bi_2O_3 and CO_2 at this temperature, forming g-C_3N_4/β - Bi_2O_3 composites; Step 4: partial β-Bi_2O_3 transfers to α-Bi_2O_3 during the cooling process due to the deprotection of g-C_3N_4 and CO_3^{2-}, while the other left β-Bi_2O_3 crystals can keep its crystal structures during this process. After these 4 steps, α-Bi_2O_3/g-C_3N_4/β-Bi_2O_3 composites were successfully constructed. This process was partially proved by the combination of TG-DTA and XRD in our earlier research[19], and supported by the XPS results in this study.

3.5 Photocatalytic Activity

The photocatalytic activities of α-Bi_2O_3/g-C_3N_4/β-Bi_2O_3 composites were evaluated by the photocatalytic oxidation of gaseous IPA under visible light irradiations. The production of acetone, the unique product of this reaction, was monitored to judge the photocatalytic activities. From Fig. 9 (A), we can see that the sample of 9.5:0.5-3h shows the highest photocatalytic activity in this reaction. The production of acetone over it is almost 1200 ppm after 8 hours' irradiation, and it is almost twice more than that over β-Bi_2O_3 (550 ppm), 5 times more than that over nano α-Bi_2O_3 (244 ppm), and 14 times more than that over g-C_3N_4 (84 ppm). Meanwhile, other α-Bi_2O_3/g-C_3N_4/β-Bi_2O_3 composite samples also shows better photocatalytic activity than the three semiconductors

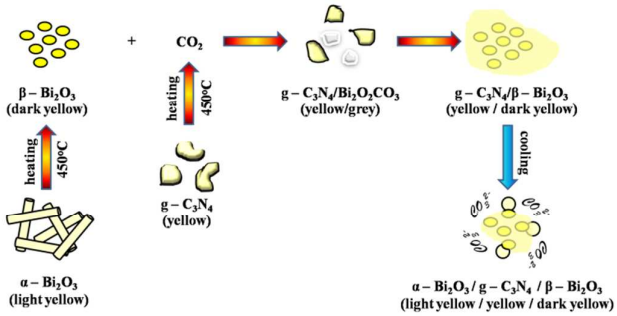

Scheme 1 The formation mechanism of α-Bi_2O_3/g-C_3N_4/β-Bi_2O_3 composite samples from α-Bi_2O_3 and g-C_3N_4.

separately, except the samples of 8.0:2.0 - 3h and 9.5:0.5 -5h. Furthermore, the oxide reaction of IPA over α-Bi_2O_3/g-C_3N_4/β-Bi_2O_3 composite (9.5:0.5 - 3h) in dark was also carried out for comparison. The result in Fig. 9 (B) shows that little acetone was produced under this condition.

We note that, β-Bi_2O_3 shows the highest photocatalytic activity in the IPA oxidation among the three semiconductors, α-Bi_2O_3, β-Bi_2O_3 and g-C_3N_4. Meanwhile, the composite sample of 9.5:0.5-4h shows the highest visible light absorption (Fig. 7), and the composite sample of 9.5:0.5-5h contains the most β-Bi_2O_3 among all the

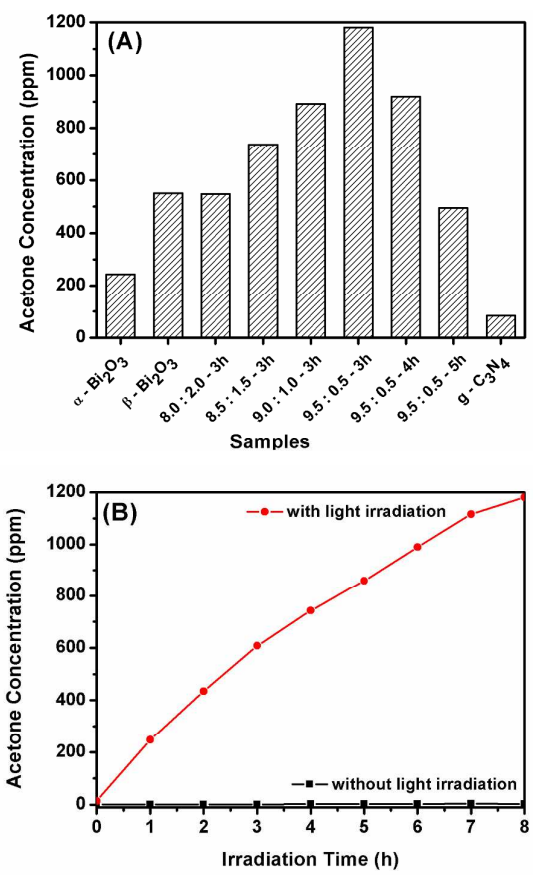

Fig. 9 (A) Photocatalytic oxidation of gaseous IPA over α-Bi_2O_3/g-C_3N_4/β-Bi_2O_3 composite samples; (B) Control experiments of the gaseous IPA oxidation

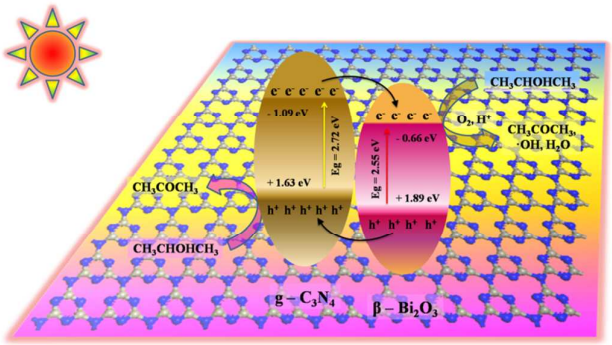

Scheme 2 The photocatalytic oxidation mechanism of IPA over α-Bi_2O_3/g-C_3N_4/β-Bi_2O_3 composite samples.

composite samples. However, both of them are not the sample with the highest photocatalytic activity, but the composite sample of 9.5:0.5-3h shows the highest photocatalytic activity. In order to explain this phenomenon, we need to investigate it in another way. When we analyzed the contents of every composite sample once again (Table 2), we got the results. From Table 1, we found that, for the composite sample of 9.5:0.5-3h, the weight ratio of g-C_3N_4 is the most, and α-Bi_2O_3 is almost negligible in this composite sample. So we think that g-C_3N_4 and β-Bi_2O_3 play the important role in the photocatalytic performance of the composite samples, and the formation of g-C_3N_4/β-Bi_2O_3 heterojunction is the crucial factor of the high photocatalytic activity.

According to the previous report, the photooxidation of IPA to acetone undergoes two typical reaction processes as follows[43-45]:

(1) h^+ oxidation : $CH_3CHOHCH_3 + h^+ \rightarrow CH_3COCH_3 + 2H^+ + e^-$

(2) O_2 oxidation : $CH_3CHOHCH_3 + e^- + O_2 + H^+ \rightarrow CH_3COCH_3 + HO\cdot + H_2O$

Therefore, the photocatalytic reaction mechanism can be described as Scheme 2. Under the visible light irradiation, both g-C_3N_4 and β-Bi_2O_3 are excited and generated the photoexcited electron and hole pairs. Since the conduction band potential of g-C_3N_4 is more negative than that of β-Bi_2O_3, the photogenerated electrons on the surface of g-C_3N_4 particles will transfer to β-Bi_2O_3. Meanwhile the photogenerated holes on the surface of β-Bi_2O_3 will transfer to g-C_3N_4, because the valence band potential of β-Bi_2O_3 is more positive than that of g-C_3N_4. These two processes are both based on the well built heterojunction between g-C_3N_4 and β-Bi_2O_3. Therefore, the photogenerated electrons and holes are separated effectively in the space, inducing a smaller possibility to recombine. Combing with the increased visible light absorption and decreased particle size of the sample, the photocatalytic activity is efficiently enhanced.

Conclusion

In conclusion, this work successfully synthesized α-Bi_2O_3/g-C_3N_4/β-Bi_2O_3 composites in one step with an in situ method from α-Bi_2O_3 and g-C_3N_4. Based on the earlier researches, the formation mechanism of α-Bi_2O_3/g-C_3N_4/β-Bi_2O_3 composites were studied and discussed in detail. The results show that CO_3^{2-} and g-C_3N_4 on the surface of β-Bi_2O_3 greatly improves its thermal stability at room temperature, inducing the formation of α-Bi_2O_3/g-C_3N_4/β-Bi_2O_3 composites. More interestingly, the photocatalytic activity for the IPA oxidation is significantly enhanced by the recombination of α-Bi_2O_3, g-C_3N_4, and β-Bi_2O_3. According to the analysis on the practical weight ratio of everyone component, the surface heterojunction between g-C_3N_4 and β-Bi_2O_3 was considered to be the main reason of the photocatalytic activity enhancement. The results and discussions in this study reveal the significant effect of g-C_3N_4 on the crystal structures and photocatalytic activity of α-Bi_2O_3.

Acknowledgements

This work was partially supportted by the National Natural Science Foundation of China (21273281), National Basic Research Program of China (973Program, No. 2013CB632405), the World Premier International Research Center Initiative (WPI Initiative) on Materials Nanoarchitectonics (MANA), MEXT, Japan, and the National Scholarship Fund.

References

1. A. Fujishima and K. Honda, *Nature*, 1972, **238**, 37-38.
2. S. J. A. Moniz, C. S. Blackman, C. J. Carmalt and G. Hyett, *J. Mater. Chem.* , 2010, **20**, 7881-7886.
3. M. Drache, P. Roussel and J.-P. Wignacour, *Chem. Rev.*, 2007, **107**, 80-96.
4. X. Lin, J. Xing, W. Wang, Z. S. F. Xu and F. Huang, *J. Phys. Chem. C*, 2007, **111**, 18288-18293.
5. M. Ge, Y. Li, L. Liu, Z. Zhou and W. Chen, *J. Phys. Chem. C*, 2011, **115**, 5220-5225.
6. H. Fan, H. Li, B. Liu, Y. Lu, T. Xie and D. Wang, *ACS Appl. Mater. Interfaces*, 2012, **4**, 4853-4857.
7. Z. Ai, Y. Huang, S. Lee and L. Zhang, *J. Alloys Compd.*, 2011, **509**, 2044-2049.
8. X. Liu, J. Liu, H. Zheng, X. Liu, G. Li and W. Zhang, *Appl. Sur. Sci.*, 2012, **258**, 4240-4245.
9. S. Anandan, G.-J. Lee, P.-K. Chen, C. Fan and J. J. Wu, *Ind. Eng. Chem. Res.*, 2010, **49**, 9729-9737.
10. A. Hameed, T. Montini, V. Gombac and P. Fornasiero, *J. Am. Chem. Soc.*, 2008, **130**, 9658-9659.
11. H. Cheng, B. Huang, J. Lu, Z. Wang, B. Xu, X. Qin, X. Zhang and Y. Dai, *Phys. Chem. Chem. Phys.*, 2010, **12**, 15468-15475.
12. M. Schlesinger, S. Schulze, M. Hietschold and M. Mehring, *Dalton Trans.*, 2013, **42**, 1047-1056.
13. J. Wang, X. Yang, K. Zhao, P. Xu, L. Zong, R. Yu, D. Wang, J. Deng, J. Chen and X. Xing, *J. Mater. Chem. A*, 2013, **1**, 9069-9074.
14. H. Y. Jiang, K. Cheng and J. Lin, *Phys. Chem. Chem. Phys.*, 2012, **14**, 12114-12121.
15. J. Eberl and H. Kisch, *Photochem. Photobiol. Sci.*, 2008, **7**, 1400-1406.
16. T. Saison, N. Chemin, C. Chan´eac, O. Durupthy, V. Ruaux, L. Mariey, F. O. Maug´e, P. Beaunier and J.-P. Jolivet, *J. Phys. Chem. C*, 2011, **115**, 5657-5666.
17. L. Zhou, W. Wang, H. Xu, S. Sun and M. Shang, *Chem. Eur. J.*, 2009, **15**, 1776-1782.
18. F. Qin, G. Li, R. Wang, J. Wu, H. Sun and R. Chen, *Chem. Eur. J.*, 2012, **18**, 16491-16497.
19. H.-Y. Jiang, G. Liu, P. Li, D. Hao, X. Meng, a. Tao Wang, J. Lin and J. Ye, *RSC Adv.*, 2014, **4**, 55062-55066.
20. D. T. Sawyer and J. S. Valentine, *Acc. Chem. Res.*, 1981, **14**, 393-400.
21. H.-Y. Jiang, G. Liu, M. Li, J. Liu, W. Sun, J. Ye and J. Lin, *Appl. Catal. B-Environ.*, 2015, **163**, 267-276.

22. Z. Bian, J. Zhu, S. Wang, Y. Cao, X. Qian and H. Li, *J. Phys. Chem. C*, 2008, **112**, 6258-6262.
23. Z. Mei, S. Ouyang, D. M. Tang, T. Kako, D. Golberg and J. Ye, *Dalton Trans.*, 2013, **42**, 2687-2690.
24. Y. Wang, X. Wang and M. Antonietti, *Angew Chem. Int. Ed.*, 2012, **51**, 68-89.
25. H. Li, J. Liu, W. Hou, N. Du, R. Zhang and X. Tao, *Appl. Catal. B-Environ.*, 2014, **160-161**, 89-97.
26. X. Wang, K. Maeda, A. Thomas, K. Takanabe, G. Xin, J. M. Carlsson, K. Domen and M. Antonietti, *Nat. Mater.*, 2008, **8**, 76-80.
27. H.-Y. Jiang, J. Liu, K. Cheng, W. Sun and J. Lin, *J. Phys. Chem. C*, 2013, **117**, 20029-20036.
28. L. Huang, H. Xu, Y. Li, X. Cheng, J. Xia, Y. Xu and G. Cai, *Dalton Trans.*, 2013, **42**, 8606-8616.
29. S. Chen, Y. Hu, L. Ji, X. Jiang and X. Fu, *Appl. Sur. Sci.*, 2014, **292**, 357-366.
30. F. Qin, H. Zhao, G. Li, H. Yang, J. Li, R. Wang, Y. Liu, J. Hu, H. Sun and R. Chen, *Nanoscale*, 2014, **6**, 5402-5409.
31. D. Barreca, F. Morazzoni, G. Andrea Rizzi, R. Scotti and E. Tondello, *Phys. Chem. Chem. Phys.*, 2001, **3**, 1743-1749.
32. H. A. Harwig, *Z. Anorg. Allg. Chem.*, 1978, **444**, 151-166.
33. P. Li, H. Xu, L. Liu, T. Kako, N. Umezawa, H. Abe and J. Ye, *J. Mater. Chem. A*, 2014, **2**, 5606-5609.
34. G. Lin, D. Tan, F. Luo, D. Chen, Q. Zhao, J. Qiu and Z. Xu, *J. Alloys Compd.*, 2010, **507**, L43-L46.
35. K. Brezesinski, R. Ostermann, P. Hartmann, J. Perlich and T. Brezesinski, *Chem. Mater.*, 2010, **22**, 3079-3085.
36. C. Li, J. Zhang and K. Liu, *Int. J. Electrochem. Sci.*, 2012, **7**, 5028-5034.
37. F. Yang, V. Kuznietsov, M. Lublow, C. Merschjann, A. Steigert, J. Klaer, A. Thomas and T. Schedel-Niedrig, *J. Mater. Chem. A*, 2013, **1**, 6407-6415.
38. P. Li, S. Ouyang, Y. Zhang, T. Kako and J. Ye, *J. Mater. Chem. A*, 2013, **1**, 1185-1191.
39. P. Madhusudan, J. Yu, W. Wang, B. Cheng and G. Liu, *Dalton Trans.*, 2012, **41**, 14345-14353.
40. H. Lu, L. Xu, B. Wei, M. Zhang, H. Gao and W. Sun, *Appl. Sur. Sci.*, 2014, **303**, 360-366.
41. X. Xiao, R. Hu, C. Liu, C. Xing, C. Qian, X. Zuo, J. Nan and L. Wang, *Appl. Catal. B-Environ.*, 2013, **140**, 433-443.
42. A. Makarowicz, C. L. Bailey, N. Weiher, E. Kemnitz, S. L. M. Schroeder, S. Mukhopadhyay, A. Wander, B. G. Searle and N. M. Harrison, *Phys. Chem. Chem. Phys.*, 2009, **11**, 5664-5673.
43. F. Arsac, D. Bianchi, J. M. Chovelon, C. Ferronato and J. M. Herrmann, *J. Phys. Chem. A*, 2006, **110**, 4202-4212.
44. Y. Ohko, K. Hashimoto and A. Fujishima, *J. Phys. Chem. A*, 1997, **101**, 8057-8062.
45. S. Ouyang and J. Ye, *J. Am. Chem. Soc.*, 2011, **133**, 7757-7763.

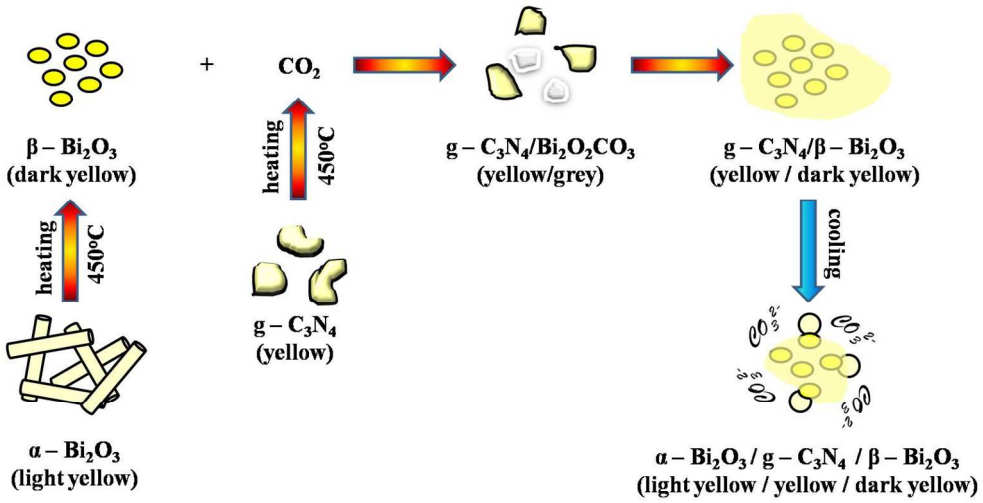

345x173mm (120 x 120 DPI)